Journal of Applied Polymer Science

Minor-Phase Particles Evolution in a Polyethylene/Ethylene-Propylene Copolymer (80/20) Blend across Mixing: Breakup and Coalescence

Xu-Huang Chen,[1] Peng Yu,[2] Sergei Kostromin,[3] Sergei Bronnikov[3]

[1]School of Chemical and Environmental Engineering, Hubei University of Technology, Wuhan 430068, PR China

[2]National Engineering Research Center of Novel Equipment for Polymer Processing, The Key Laboratory of Polymer Processing of Ministry of Education, South China University of Technology, Guangzhou 510640, PR China

[3]Russian Academy of Science, Institute of Macromolecular Compounds, Bolshoi Prospekt 31, Sankt Petersburg 199004, Russian Federation

Correspondence to: S. Bronnikov (E-mail: bronnik@hq.macro.ru)

ABSTRACT: On the basis of an online sampling microscopy method, the morphological evolution of a metallocene polyethylene/metallocene ethylene–propylene copolymer system (80/20 vol %) across various mixing regimes was investigated and treated statistically. The size distributions of the minor-phase metallocene ethylene–propylene (mEP) droplets were described with principles of irreversible thermodynamics. Such an approach allowed us to find two superimposed statistical ensembles involving primary (broken) and secondary (coalesced) mEP particles. The mean size and relative number of both broken and coalesced mEP particles were calculated. The evolution of these characteristics across melt mixing, static coalescence, and flow-driven coalescence was analyzed. © 2013 Wiley Periodicals, Inc. J. Appl. Polym. Sci. 130: 3421–3431, 2013

KEYWORDS: blends; microscopy; morphology; phase behavior; polyolefins

Received 6 December 2012; accepted 1 April 2013; Published online 23 June 2013
DOI: 10.1002/app.39373

INTRODUCTION

There has been a long-standing interest from polymer researchers in understanding the formation and evolution of blend morphology, which has a significant influence on mechanical properties.[1–5] During the past few decades, many research groups have carried out studies to gain a better understanding of the morphological development of polymer blends across mixing.[6–17] It is well known that the morphology of polymer blends is mainly determined by two dynamic processes, breakup and coalescence. A stable structure is obtained when the dynamic equilibrium between the breakup and coalescence of dispersed phase is approached under shear. Plochocki et al.[7] studied the dependence of the domain morphology on industrial mixing processes carried out on low-density polyethylene/polystyrene (PS) mixtures; they proposed that an abrasion mechanism is responsible for the early stage of the dispersion process and that the final domain size is controlled by a breakup–coalescence equilibrium. Scott and coworkers[8,10,11,14] proposed a mechanism for the initial morphological development of polymer blends that involves the formation of sheets or ribbons of the dispersed phase in the matrix, which are drawn out of a large mass of the dispersed phase. Because of interfacial and flow forces, holes form in the ribbon and grow until a lace structure is formed. This lace is then broken down into irregularly shaped particles and finally into nearly spherical particles. This mechanism results in the generation of very small particles in very short timescales.

Along with blending processes, the dispersed domain size becomes increasingly smaller, and thus breakup is suppressed; furthermore, a shear stress decrease in the late mixing stage induces coalescence because of an increase in the effective collision probability between the dispersed particles. So, the final morphology and interfacial properties are particularly sensitive to coalescence phenomena, which can be divided into two broad categories: static coalescence and dynamic coalescence. In the former, the aggregation of dispersed particles can be caused by a multiphase polymer's annealing under molten status. The thermodynamic reason responsible for this coarsening is a reduction in the interfacial area or interfacial energy.[18] Traditionally, the coarsening behavior can be described by the Ostwald ripening mechanism[19,20] and the Brownian coagulation mechanism.[21,22]

Both mechanisms yield the same relation between the mean particle radius (R) and the annealing time (t):

$$R^3 = R_0^3 + Kt$$

where R_0 is the initial radius at $t = 0$ and K is the rate constant. It is believed that during coarsening, both Brownian-particle motion-driven coalescence and molecular-diffusion-driven Ostwald ripening can operate at the same time, and their relative importance depends on the hydrodynamic and thermodynamic conditions. In fact, predictions often give values two or three orders of magnitude lower than experimentally observed coarsening rates.[23] Hu et al.[18] developed a model that considered for the first time that coarsening is driven by van der Waal's forces and that there is slippage at the interfacial boundaries between the moving particles and the matrix. Fortelny and coworkers[24–27] considered another coalescence mechanism that could be divided into four stages: particle approach, film draining, film rupture, and neck relaxation. They took the film-drainage time as the coalescence time between two particles. This mechanism predicts a coalescence that is substantially quicker than the mechanism determined experimentally. In the real coalescence processes, the rate-control step may not be the same for different systems. Therefore, Zhou et al.[28,29] combined all factors to propose a new coalescence model describing the coarsening behavior of immiscible polymer blends. The predictions of the model were in good agreement with the experimental data.

Dispersed particles would be aggregated because of the polymer's shear flow under certain flow conditions. Flow-driven coalescence actually is simpler to model than static coalescence; moreover, it is more practical to consider the flow-driven coalescence, which concurs with dispersed particle breakup. Consequently, studies about the coalescence during shear are attracting more interest from both academic and commercial institutes. Vinckier et al.[30] reported a flow-driven coalescence with a polybutadiene/polydimethylsiloxane system. Kim et al.[31] studied coalescence in poly(styrene-*co*-acrylonitrile)/poly(cyclohexyl methacrylate) blends compatibilized with PS-*block*-poly(methyl methacrylate). Lyu et al.[32,33] reported studies of a PS/high-density polyethylene system. Rusu and Peuvrel-Disdier[34] and Börschig et al.[35] also reported investigations of particle coalescence. Li et al.[36] studied the shear-induced coalescence of particles in polypropylene/PS blends with different compositions. All of these researchers used similar methods: coalescence was monitored after a step down in shear rate. These blend samples were presheared at higher rates to form smaller and relatively uniformer particle morphologies. This ensured that the flow-driven coalescence was separated from breakup. In addition, all of these investigations reached two common conclusions: the coalescence rate increased with increasing particle concentration, and coalescence efficiency decreased with increasing shear rate. These could be qualitatively explained, in the former case by an increased number of collisions according to ideal collision mechanism[37] and in the latter case in terms of particle deformation that caused a greater resistant force to coalescence in reference to matrix film-drainage theory.[38] Furthermore, Lyu et al.[32] found that the coalescence efficiency decreased when the particle sizes differed. This result directly confirmed the importance of hydrodynamic interactions between particles due to trajectories, as proposed by Zeichner and Schowalter[39] and Wang et al.[40]

Theoretical studies of blend morphology mainly involve the establishment of numerical models to predict the variation of particle size as a function of blending time and the mathematical behaviors during blending. Experimental studies concerning the morphology of particles during blending make it more convenient to verify the theories of morphology evolution and improve those models further. Unfortunately, some results are not consistent because of differences in the polymer blends studied; these indicate that the mechanism of morphological evolution might depend greatly on the specific blend system, such as immiscible and compatible blend systems. Thus, it is meaningful to further study the morphological evolution in other polymer blends that are different from those discussed earlier.

In this study, the phase formation and evolution of a metallocene polyethylene/metallocene ethylene–propylene copolymer (mPE/mEP) system were investigated. Polyethylenes are plastic materials with the most diversified uses in industry, and the newest member of this family is a polyethylene synthesized by constrained geometry metallocene catalyst technology. This new class of polyethylene exhibits a molecular structure with a narrow molecular-weight distribution and a uniformity of comonomer distribution and often offers unique mechanical and rheological properties. However, metallocene polyethylene (mPE) has poor processability because of its high viscosity, whereas metallocene ethylene–propylene (mEP) is an elastomer that can be widely used to toughen olefinic polymers, such as polypropylene and polyethylene.[17]

On the basis of the image analysis of scanning electron microscopy (SEM) patterns, the phase formation and evolution of the mPE/mEP system were investigated. The statistical size distributions of the minor-phase particle size during melt mixing and their consequent analytical description with principles of irreversible thermodynamics allowed us to find ensembles of broken and coalesced particles, estimate their mean diameters, and plot their evolution with mixing time. Furthermore, the static coalescence and flow-driven coalescence were also studied as functions of time, respectively, to understand the evolution of the morphological development under quiescent annealing and low-shear-rate flow conditions.

EXPERIMENTAL

Materials

mPE (Exxon-2018CA) was a commercial polymer from Mobil Oil Corp. [density = 0.918 g/cm^3 and melt index = 2.0 g/10 min (2.16 kg, 230°C)]. The elastomer, a copolymer of ethylene and propylene synthesized with a metallocene catalyst (mEP, VMX-6202), was a commercial material from Mobil Oil Corp. [density = 0.861 g/cm^3 and melt index = 7.4 g/10 min (2.16 kg, 190°C)].

Sample Preparation

Before blending, both materials were heated at 80°C *in vacuo* for 24 h to remove any volatiles. The selected composition for

Table I. Chosen Coalescence Times of the mPE/mEP (80/20 vol %) Blend

Coalescence category	Coalescence time (min)									
Static coalescence	0	10	120	180	240	360	420	480	540	600
Flow-driven coalescence	0	1	2	5	10	60	120	180	240	300

the mPE/mEP blending was 80/20 vol %. The binary blending of mPE and mEP was done by melt-mixing the components in a mixing apparatus (SU-70 internal mixer, Zhangjiagang Lanhang Machinery Co., Ltd., China) at a temperature of 180°C with a rotational speed of 36 rpm; the volume of material in the mixer at the operating temperature was kept at 60 cm^3. A sample of around 2 g was taken from the indents of the mixer blades at different mixing time intervals (0.5, 0.75, 1, 1.5, 2, 3, 4, 6, 8, and 10 min) and was immediately quenched in liquid nitrogen. This allowed us to study the evolution of the blend morphology over time during melt mixing.

In addition, two regimes of coalescence, namely, static coalescence and flow-driven coalescence, were studied in this work. To probe the size of the dispersed phase during the coalescence, a flow procedure corresponding to a step down in shear rate was applied. An mPE/mEP (80/20 vol %) blend was first mixed in the aforementioned batch internal mixer at 180°C with a rotational speed of 36 rpm for 10 min to obtain a fine morphology. Subsequently, the rotor speed was stopped and reduced to 1 rpm, respectively, to induce coalescence; this corresponded to static coalescence and flow-driven coalescence. This lower shear rate (1 rpm) ensured that the subsequent morphological development was dominated by a coalescence mechanism. To examine the morphological development during coalescence, samples at different coalescence times (shown in Table I) were taken out of the mixer and were then rapidly quenched in liquid nitrogen to freeze the original structure for SEM observation.

Morphological Characterization

The morphologies of the blends were observed under a scanning electron microscope (6390 LV, JEOL JSM, Japan) at an accelerating voltage of 20 kV and a magnification of 5000. The cryofractured surface of each specimen was etched by cyclohexane at room temperature for 30 min to remove the mEP phase. Then, the fracture surfaces of the specimens were coated with a thin layer of gold for microscopic observation to ensure that the etched surface structure of the blends was intact.

The SEM images obtained were subsequently segmented and subjected to digital analysis with our homemade processing software[15,17] to elucidate the statistical size distribution of the minor-phase particles. To analytically describe the resulting histograms and find the mean diameter of the dispersed-phase particles, we used the model of reversible aggregation.

MODEL

The model of reversible aggregation[41,42] is inspired by application of irreversible thermodynamics. It gives a generalized characterization of microstructure in liquids. According to the model, a stationary microstructure is developed by the linking of the energy-equivalent units in metastable clusters called *aggregates*. The aggregates are permanently composed and decomposed under thermal fluctuations; this is a condition of their reversibility. The universality of the model has been demonstrated by its application to statistical ensembles of morphological entities of different nature (polymers, liquid crystals, carbon black, bacteria, yeast, etc.) across their transformation in chemical and physical processes (see refs. 41–43 and references therein). Recently, the model has been successfully applied to the analysis of polymer blend morphology.[44–46]

According to the model, the stationary statistical distribution $[h(s)]$ of the planar size (s) of the microstructural entities can be calculated as follows:[41,42]

$$h(s)=as^2\exp\left(-\frac{s\Delta u_0}{kT}\right) \tag{1}$$

where a is the normalizing factor, Δu_0 is the aggregate energy, k is the Boltzmann constant, and T is the absolute temperature. The Δu_0 parameter can be interpreted as a potential barrier to be overcome to form a statistical ensemble. As the process is controlled by thermal fluctuations, Δu_0 should rather be compared with the energy of the thermal fluctuation (kT).

In some cases, the aggregates were shown to form not a single but rather multiple statistical ensembles.[44,46] This may be caused by the consolidation of primary entities into a novel superstructure (i.e., coalescence). In this way, eq. (1) should be written as[43,44,46]

$$h(s)=\sum_{i=1}^{N} a_i s_i^2\exp\left(-\frac{s_i\Delta u_{0i}}{kT}\right) \tag{2}$$

where index i accounts the number of a statistical ensemble and N is the total number of statistical ensembles of the entities. Equation (2) allows the determination of the mean entity area $(\langle s_i\rangle)$ related to the ith statistical ensemble as a normalized mathematical expectation:

$$\langle s_i\rangle=\frac{\int_0^\infty s_i^2\exp\left(-\frac{s_i\Delta u_{0i}}{kT}\right)ds_i}{\int_{0_{0i}}^\infty s_i^2\exp\left(-\frac{s_i\Delta u_{0i}}{kT}\right)ds_i}=\frac{3kT}{\Delta u_{0i}} \tag{3}$$

The relation between the linear (diameter $\langle d_i\rangle$) and planar area $(\langle s_i\rangle)$ mean size of the entities of a circular shape in the ith ensemble is then given by a simple geometrical regulation:

$$\langle d_i\rangle=2\sqrt{\frac{\langle s_i\rangle}{\pi}} \tag{4}$$

If the entities have a noncircular shape, both $\langle d_i\rangle$ and $\langle s_i\rangle$ should be treated rather as the effective mean parameters.

The ratio R between the numbers of entities involved in the mth and nth statistical ensembles (N_m and N_n, respectively) can be estimated with a relation between the integral characteristics:

$$R=\frac{N_m}{N_n}=\frac{\int_0^\infty s_m^2 \exp\left(-\frac{s_m \Delta u_{0m}}{kT}\right) ds_m}{\int_0^\infty s_n^2 \exp\left(-\frac{s_n \Delta u_{0n}}{kT}\right) ds_n}. \quad (5)$$

where s_m and s_n are the mean entity areas related to the m^{th} and n^{th} statistical ensembles, respectively.

RESULTS AND DISCUSSION

Evolution of the Phase Morphology During Melt Mixing

The typical morphologies of the mPE/mEP (80/20 vol %) blend at different melt-mixing times are shown as examples in Figure 1. The etching of the microscopically fractured surfaces of the alloys with cyclohexane removed the elastomer (mEP) component and left "black holes" surrounded by the mPE matrix. This is shown directly in Figure 1(a), where large and irregular shaped particles of the dispersed phase were formed at the beginning of mixing. Along with the blending progress, the dispersed particle size gradually decreased and the shape of particles also became uniform [Figure 1(b)]. After 2 min of mixing, spherical and ellipsoidal cavities were observed to distribute uniformly throughout the sample; meanwhile, the particle size became stable basically [Figure 1(c)]. The results illustrate qualitatively that the change in the phase structure mainly occurred in the initial stage of polymer blending, and this corresponded to the mechanism for the initial morphological development in polymer blends proposed by Scott and coworkers.[8,10,11] For sea-islands structure in multiphase polymer blends, the dispersed particle size plays a significant role in the characterization of the phase morphology.

Figure 2 shows histograms resulting from the statistical analysis of the SEM micrographs. To analytically describe the histograms, we used the model of reversible aggregation.

To quantitatively estimate the analytical description adequacy, we calculated the error parameter (Δ) as follows:

$$\Delta=\frac{|A_m-A_e|}{A_e} \quad (6)$$

where $A_e=\sum_{j=1}^{n} h_j s_j$ is the total area of the experimental statistical bars in a histogram (h_j and s_j are the height and the width of the jth bar, respectively, and n is the total number of bars), that is, the total area of the minor phase in a micrograph found experimentally, and $A_m=\int_0^s h(s)ds$ is the area under the curve $h(s)$, that is, the total area of the minor-phase particles in a micrograph computed analytically with eq. (1) or (2). Of course, Δ could be a reliable criterion when the maximum position is the same for both the experimental histogram and analytical function.

Our attempt to describe the statistical size distributions shown in Figure 2 with a one-component version of the model [eq. (1)] failed because Δ was as large as 35–47%. However, we succeeded when we applied a bicomponent version [eq. (2), $N=2$] with the fitting parameters listed inside the boxes, along with the mean droplet diameters computed with eqs. (3) and (4). The low Δ values (0.5–12%) also shown in the boxes is a criterion of eq. (2) applicability for the analytical description of the histograms and the accurate position of two statistical ensembles in a histogram. In Figure 2, the thin lines represent individual ensembles, whereas the thick lines represent the sum over two ensembles according to eq. (2). A successful analytical description indicated that the particles of the mEP phase formed two superimposed thermodynamically optimized statistical ensembles of primary and secondary particles all across the mixing of the mPE/mEP components. We attributed the

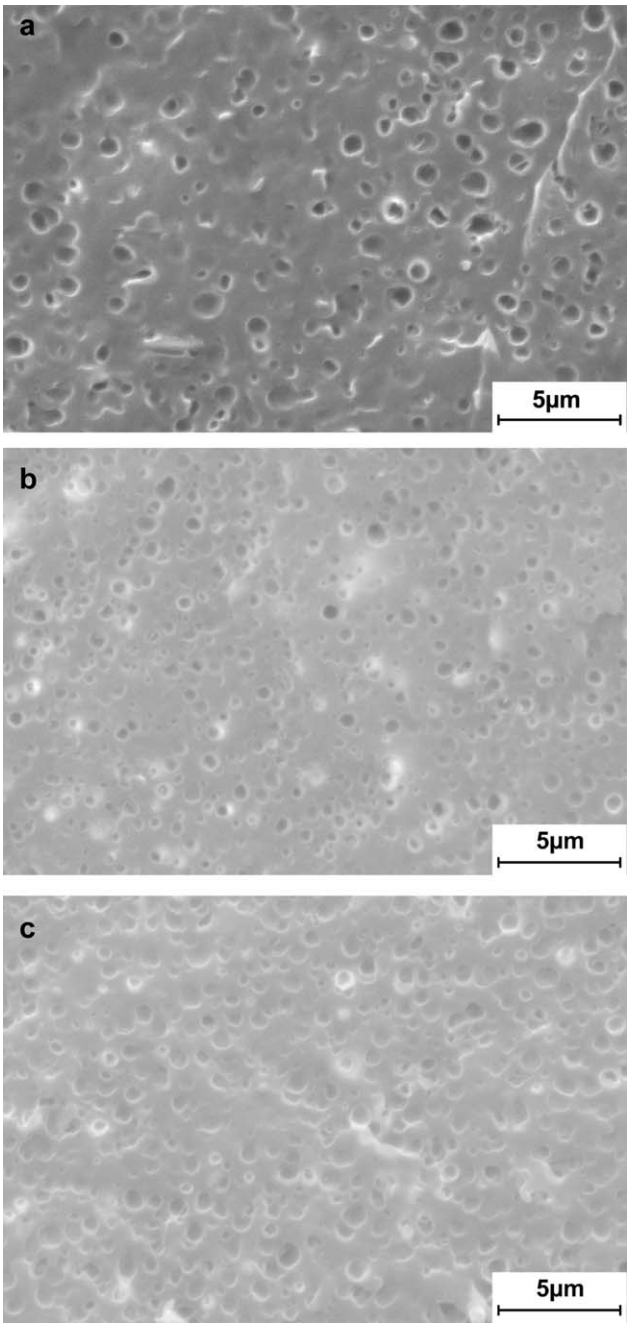

Figure 1. SEM images of the mPE/mEP blend during melt mixing at (a) 0.75, (b) 2, and (c) 8 min.

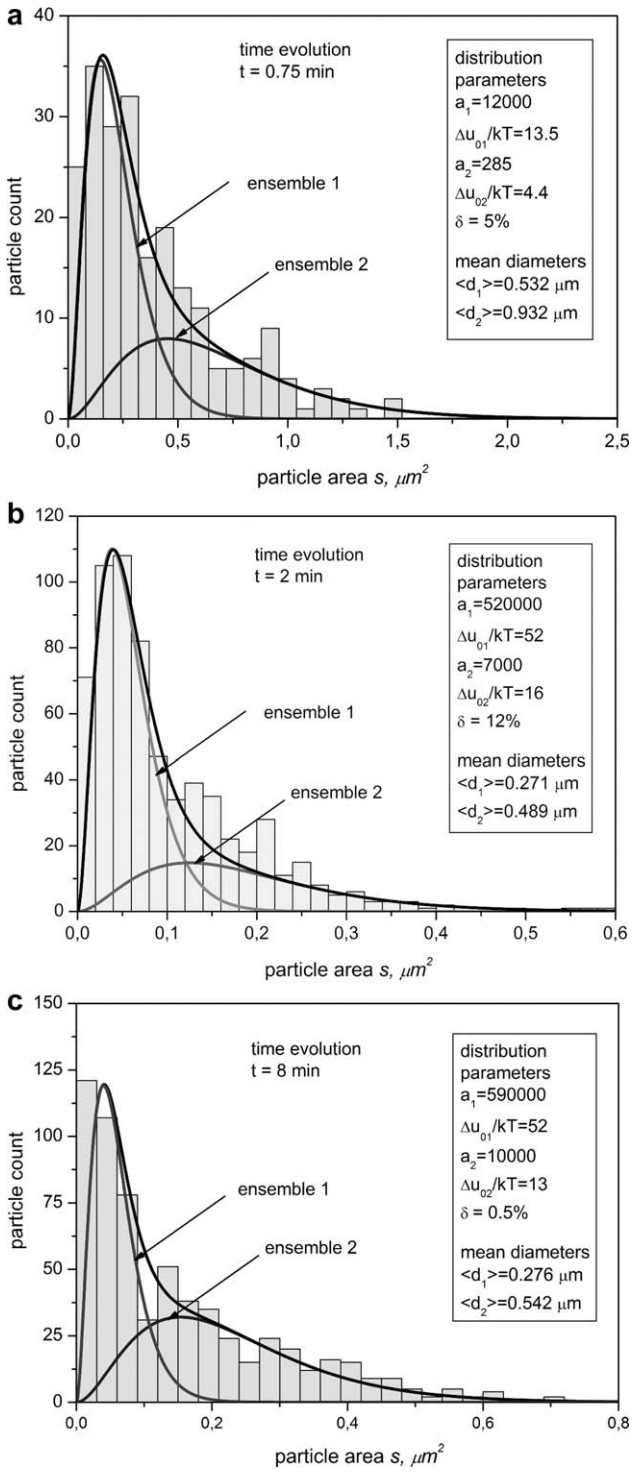

Figure 2. Statistical area distributions of the mEP phase particles of the mPE/mEP blend during melt mixing at (a) 0.75, (b) 2, and (c) 8 min.

existence of two statistical ensembles of the minor phase to two compulsory regimes of the minor-phase evolution: breakup and coalescence, both of which are typical for the mixture of incompatible polymers.[44,46]

Figure 3 shows evolution of the mean diameters of the minor-phase particles belonging to both statistical ensembles with mixing time. The whole melt-mixing process could be divided into three regions, which were interpreted as follows. At the beginning of mixing (within 1 min), the mean diameters of the particles belonging to both statistical ensembles decreased sharply (region I). According to Elemans et al.,[9] the particles of the dispersed phase were broken up and converted to smaller particles during this initial stage of the mixing. From a thermodynamic point of view, a decrease in the particle mean size indicated an increase in the potential barrier (Δu_0) to be overcome for the formation of a statistical ensemble [see eq. (1)]. We concluded that at the beginning of mixing, the formation of the statistical ensembles of both broken and coalesced particles was hindered over the course of time. In region II, a short intermediate mixing stage, the mean size of the dispersed phase particles in both statistical ensembles increased slowly with increasing mixing time. In this mixing stage, there was an increased probability of effective collision between particles as the number of the broken particles increased significantly (see the discussion of Figure 4 later). Thermodynamically, this regime can be interpreted as a decrease in the potential barrier [Δu_0 (see eq. (1)]. In the late mixing stage (after 3 min), both the breakup and coalescence of the dispersed phase particles came to a dynamic equilibrium gradually (region III). Thus, the morphology of the dispersed phase was almost unchangeable in region III. These results imply that the phase morphology mainly formed at the initial stage, that is, within 2 min after the beginning of melt mixing.

The ratio between numbers of particles involved in the first (N_1) and in the second (N_2) statistical ensembles was computed with eq. (5) and is depicted in Figure 4. This demonstrated a general decreasing tendency of the number of broken particles because of their coalescence with time. A detailed analysis of Figure 4 allowed us to find a short intermediate regime (between 1 and 2 min) where the number of broken particles increased significantly because of effective mixing. This regime can also be seen in Figure 3.

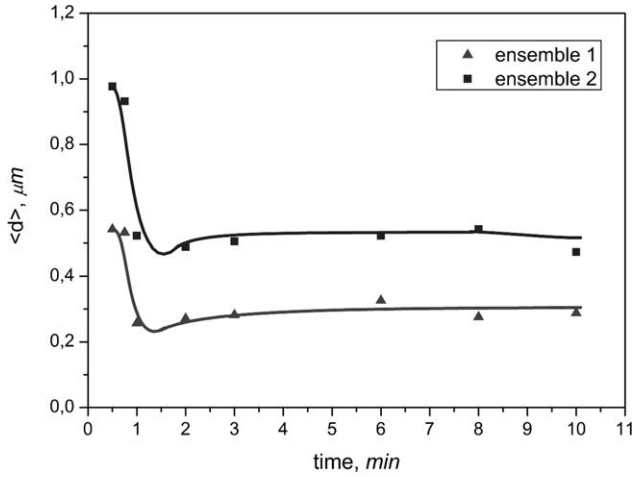

Figure 3. Variation of the mean diameter of the broken and coalesced mEP phase particles with mixing time during the melt mixing of the mPE/mEP blend.

Applied Polymer SCIENCE

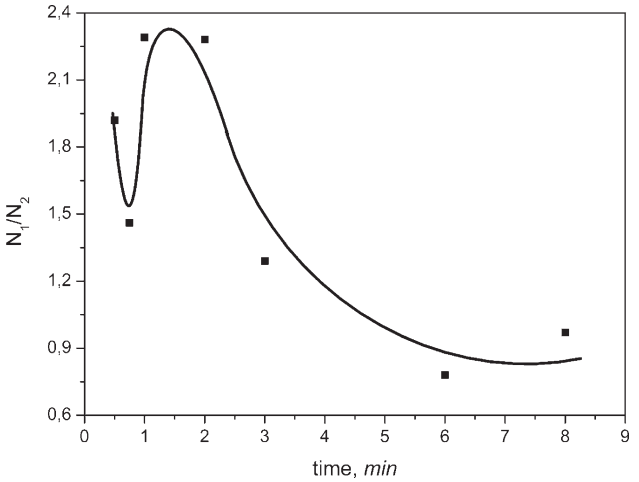

Figure 4. Variation of the ratio R between the numbers of broken and coalesced mEP phase particles with mixing time during the melt mixing of the mPE/mEP blend.

Particle Size Evolution During Quiescent Coalescence

Figure 5 shows the SEM micrographs of the mPE/mEP (80/20 vol %) blend at different quiescent coalescence times. We observed qualitatively from the SEM micrographs that the size of the dispersed particles increased gradually with coalescence time; at the same time, the number of dispersed particles decreased by degrees. The blend maintained a sea-islands morphology during the whole coalescence process, whereas the shape of the dispersed particles ranged from spherical to ellipsoidal or irregular. Meanwhile, particle size uniformity became poorer; there was the coexistence of large particles and much smaller particles because of different coalescence efficiencies between particles of different sizes.[32,47] Neighboring particles aggregated and merged into larger particles under the effect of interfacial tension (Γ). However, the coalescence efficiency between similar sized particles was superior to that between particles with distinct differences in size. Consequently, these large particles with prior coalescence abandoned circumambient small particles and continued to merge with counterparts of their size as a result of the discontinuity of particle size distribution.

Figure 6 depicts histograms resulting from a statistical analysis of the SEM micrographs. We successfully described the histograms with a bicomponent version [eq. (2), $N = 2$] within the time interval between 0 and 420 min. This allowed to find two compulsory regimes of the minor-phase evolution: breakup and coalescence. However, the histograms obtained at 420 and 600 min could be fairly described with a one-component version of the model [eq. (1), $\Delta = 17\%$] rather than with a bicomponent version [eq. (2), $\Delta = 38\%$]. This means that the primary (broken) particles disappeared because of their total coalescence.

Figure 7 shows variation of the mean diameters of the minor-phase particles of the mPE/mEP blend computed with eqs. (3) and (4) at different quiescent coalescence times. As shown, the mean diameters of both the broken and coalesced particles increased with the extension of the quiescent coalescence time up to 300 min but at different rates; the mean diameter of the broken particles increased a bit (from 0.30 to 0.56 μm), whereas the mean diameter of the coalesced particles increased three times (from 0.45 to 1.52 μm). However, in the late stage of coalescence (after about 350 min), the coalesced particle size decreased, and broken particles disappeared completely. The mean-diameter variation tendency could be explained via a static coalescence mechanism proposed by Fortelny et al.[24–27] At the beginning of coalescence, the small size and large number of primary (broken) particles, large interfacial area (or high interfacial energy), and high probability of collision between the primary particles resulted in fast coalescence and hence a great

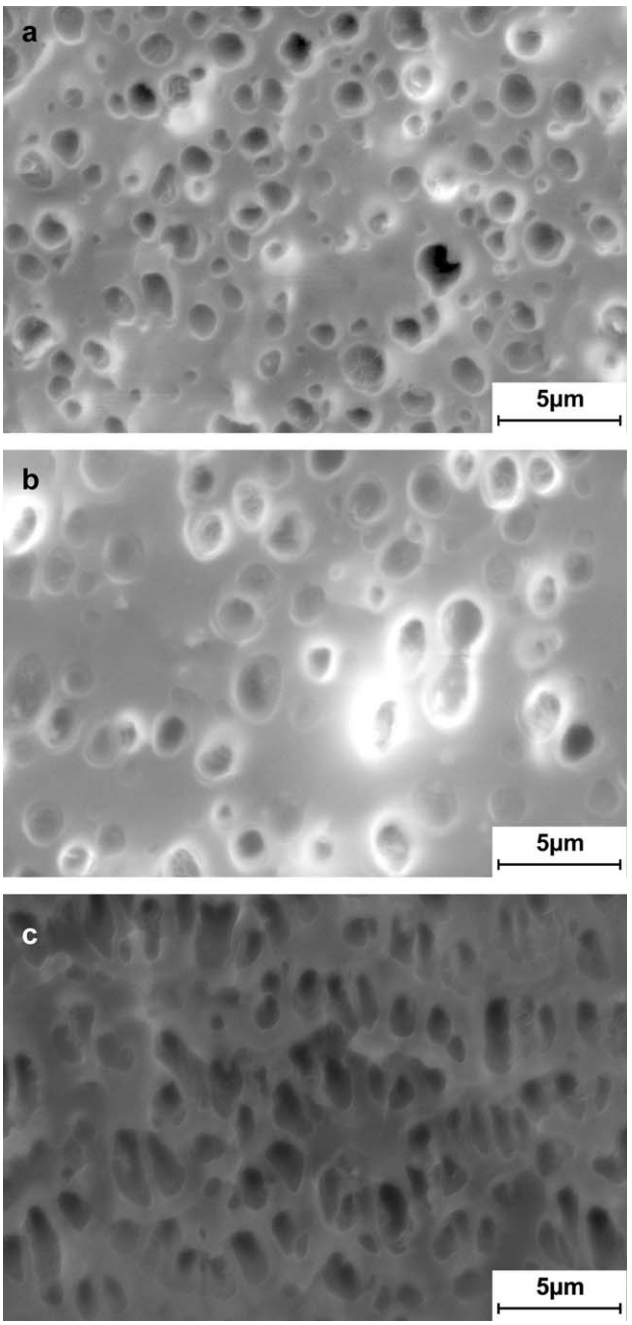

Figure 5. SEM images of the mPE/mEP blend during quiescent coalescence at (a) 60, (b) 240, and (c) 420 min.

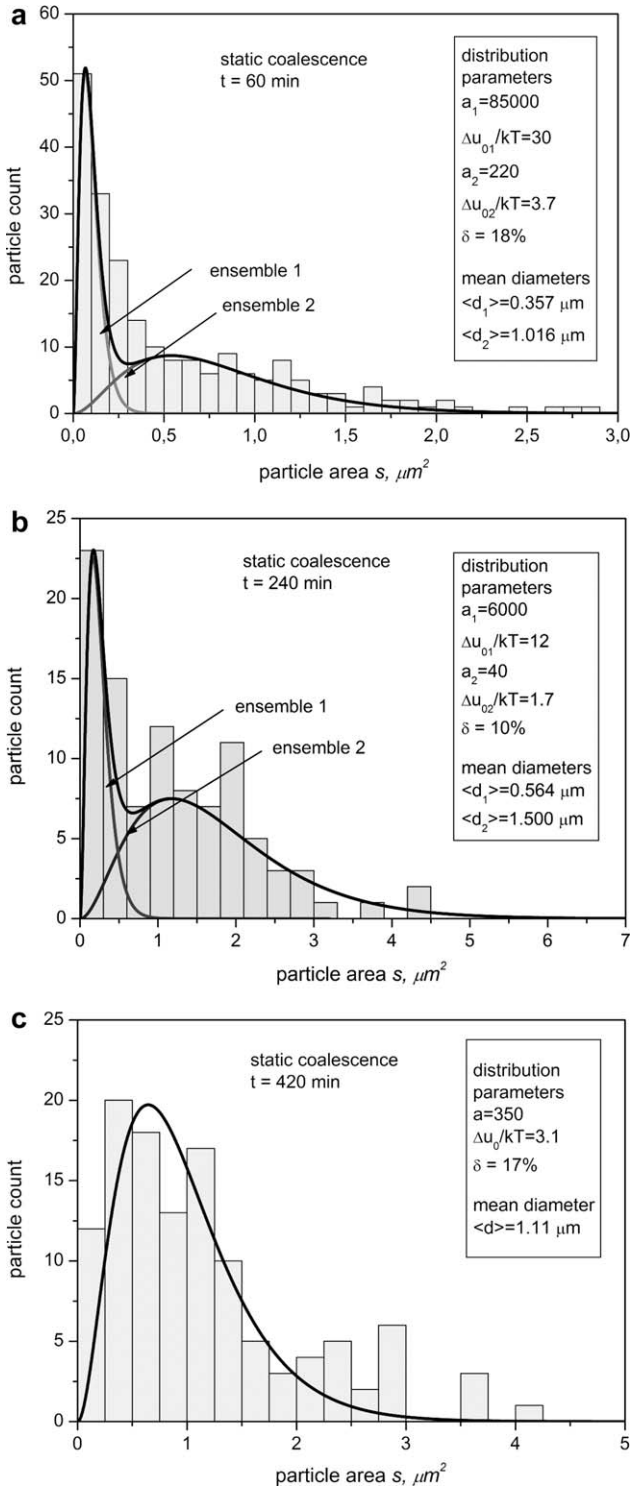

Figure 6. Statistical area distributions of the mEP phase particles of the mPE/mEP blend during quiescent coalescence at (a) 60, (b) 240, and (c) 420 min.

increment in the coalesced particle size. Coalesced particles were produced through adjacent broken particle merging, which increased the coalesced particle size and decreased the broken particle number (see later discussion). Thus, the critical matrix film thickness (h_c) between two particles increased; this corresponded to an increase in the time required for the drainage of the matrix films; this was considered the control step. So, the coalescence efficiency decreased, and the coalesced particle size increased slowly in the middle stage of coalescence; this was demonstrated by an observation of dumbbell-like particles from the SEM micrographs. Noticeably, a declining tendency after about 350 min was observed, which was probably due to the mPE crosslinking at a high temperature for a heating time that was too long (600 min) in the mixer.

An increase in the mean diameter of the broken particles with time in the absence of a strong flow field seemed at first to be a surprising phenomenon. However, we needed to take into account a dramatic decrease in the relative number of broken particles with time (see later discussion) because of their coalescence. Presumably, the smallest broken particles coalesced exceptionally. After coalescence, they left the ensemble of broken particles and came to the ensemble of coalesced particles. That is why the mean size of broken particles increased with time slowly up to 350 min. However, finally, all of the broken particles disappeared because of their intensive coalescence.

Figure 8 depicts the variation of R during static coalescence. R rapidly decreased (presumably in a linear manner) because more and more primary dispersed particles coalesced, and finally, above 400 min, all of the particles of the minor phase were coalesced.

Particle Size Evolution During Flow-Driven Coalescence

Figure 9 shows typical SEM micrographs of the mPE/mEP (80/20 vol %) blend at different shear-induced coalescence times. As expected, the dispersed particles size increased, and, in other words, the number of particles decreased during the coalescence process. The blend presented a matrix particle morphology with mEP being the dispersed phase, whose morphological changes from spherical particles in the initial stage (0–10 min) to ellipsoidal or irregular particles in the later stages (60–300 min). At the same time, the structure of broken and coalesced particle coexistence was observed. We also observed that dumbbell-like

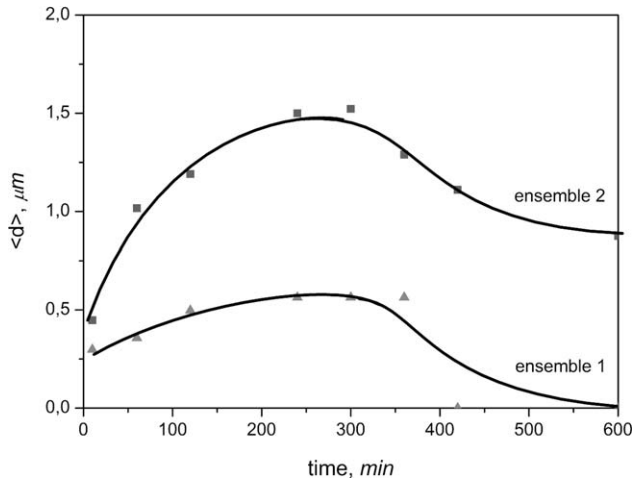

Figure 7. Variation of the mean diameter of the broken and coalesced mEP phase particles of the mPE/mEP blend with time during quiescent coalescence.

Applied Polymer SCIENCE

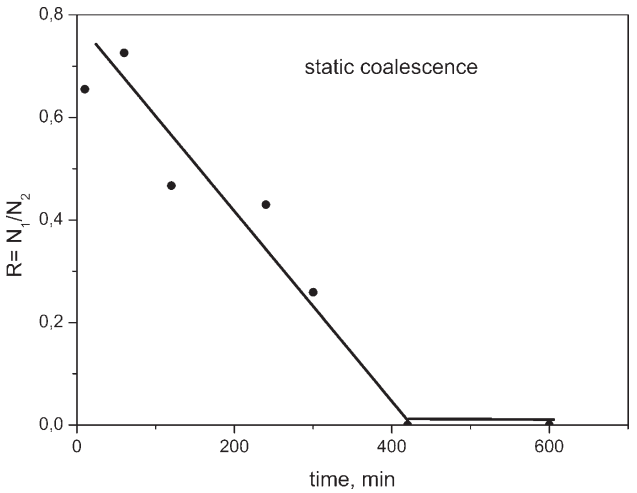

Figure 8. Variation of the ratio R between the numbers of broken and coalesced mEP phase particles with time during quiescent coalescence.

particles appeared in the later coalescence stages; this illustrated the drainage of matrix films between neighboring particles, which indirectly indicated that the coalescence rate decreased in the later stages.

Figure 10 presents the histograms obtained from statistical analysis of the SEM micrographs. They were successfully described with a bicomponent version [eq. (2), $N = 2$] within the entire time interval studied. This means that two statistical ensembles of primary (broken) particles and secondary (coalesced) particles coexisted all across the flow-driven regime corresponding to a rotor speed of 1 rpm. This speed did not seems to be great enough to suppress the coalescence of the minor-phase particles.

The relation between the mean diameter and dynamic coalescence time is also studied as shown in Figure 11. We observed that the mean diameters of dispersed particles involved in two statistical ensembles increased with increasing dynamic coalescence time. However, there were differences in the incremental amplitudes of the mean particle diameter at different coalescence moments. In the initial stage (0–10 min), the mean diameters of the particles involved in both statistical ensembles increased rapidly from 0.28 μm (the first ensemble) and 0.54 μm (the second ensemble) at 0 min to 0.67 and 1.42 μm, respectively, at 10 min. This indicated that both the breakup and coalescence rates were fast in the initial stage, whereas in the later stage, the mean diameters in both ensembles increased slowly. The matrix film-drainage theory proposed by Chesters[39] and Janssen and Meijer[48] could be used to explain the variation tendency of the mean diameter of the dispersed particles. We assumed that coalescence occurred when the gap between two particles reached h_c, at which time the matrix film between the particles automatically ruptured. Theoretical research shows that

$$h_c = (A\bar{D}/16\pi\Gamma)^{1/3}$$

where A is the Hamaker constant and $\bar{D}$ is the average particle diameter. In the initial stage, $\bar{D}$ was small, and this led to a small h_c. Moreover, the collision probability was high because of the large number of primary (broken) particles. The two factors determined a faster coalescence rate in the initial stage. As the coalescence process continued, neighboring primary particles aggregated with other and merged into larger particles; this resulted in increases in the dispersed particle diameter and h_c and a reduction in the collision probability because of a decrease in the particle numbers, so the coalescence rate decreased in the later stages.

Again, an increase in the mean diameter of the broken droplets with time could be explained by the exceptional coalescence of

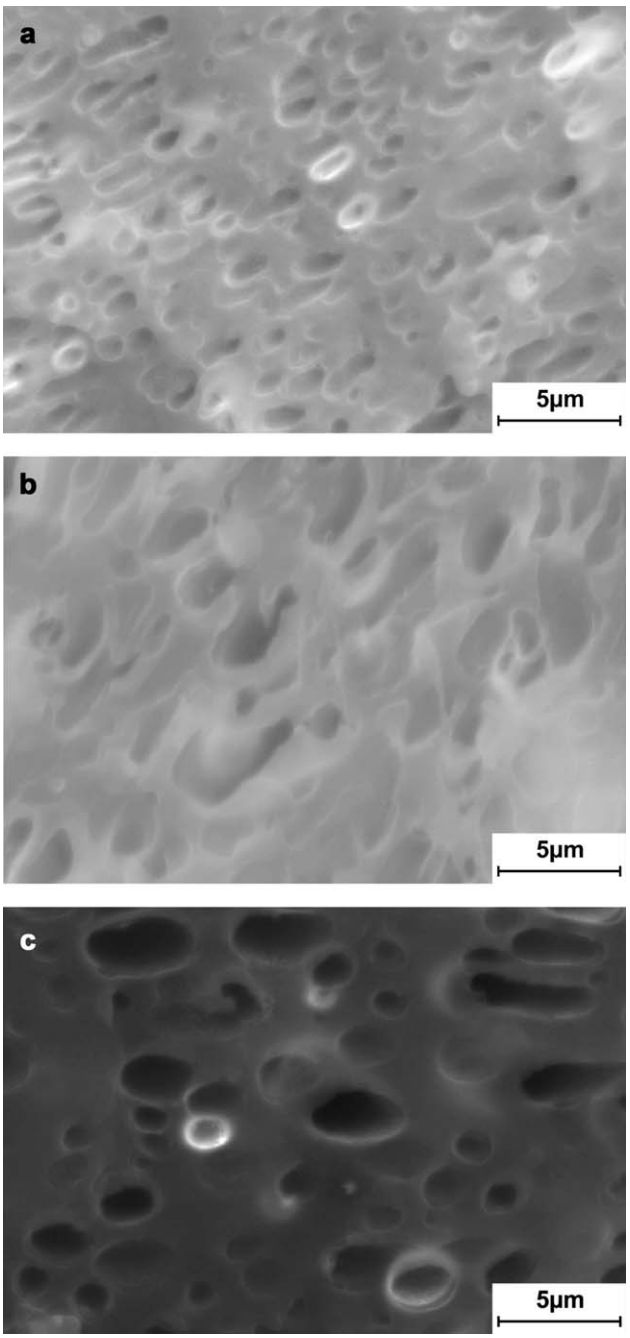

Figure 9. SEM images of the mPE/mEP blend during dynamic coalescence at (a) 1, (b) 60, and (c) 240 min.

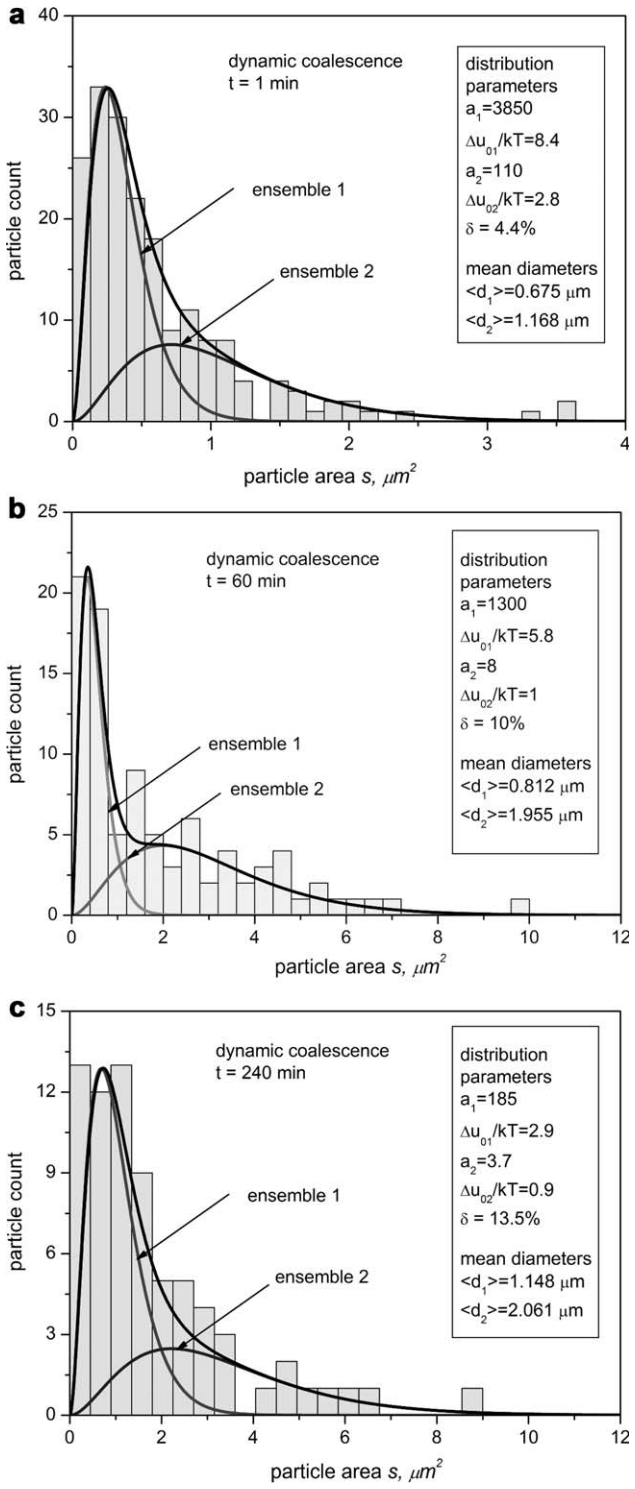

Figure 10. Statistical area distributions of the mEP phase particles of the mPE/mEP blend during dynamic coalescence at (a) 1, (b) 60, and (c) 240 min.

the smallest broken particles, their transference to the ensemble of coalesced particles, and therefore the exhaustion of small particles in the ensemble of broken particles.

The behavior of the minor-phase particles across flow-driven coalescence is also reflected in Figure 12, which shows the variation of R between N_1 and N_2 with time. In the initial stage, R decreased because of the intensive coalescence and achieved a minimum value at about 60 min. In the later stage, R increased and achieves a maximum value at about 130 min. However, in the latest stage, R decreased again because of intensive coalescence.

CONCLUSIONS

In this study, the morphological evolution of an mPE/mEP (80/20 vol %) blend across various mixing regimes was investigated with an online sampling microscopy method. Statistical image analysis and consequent thermodynamic description allowed us to find two superimposed statistical ensembles involving primary (broken) and coalesced (secondary) particles of the minor component (mPE) and to analyze the evolution of their mean size and the relative number of particles across mixing, static coalescence, and dynamic coalescence.

In the regime of intensive mixing, the mean size of both the broken and coalesced mEP particles initially (<1 min) decreases sharply, then (between 1 and 2 min) increased slowly, and finally (>3 min) achieved a dynamic equilibrium. In the regime of static coalescence, the mean size of both broken and coalesced mEP particles increased, achieved a maximum (at about 300 min), and decreased a bit; across the regime, the relative number of broken particles decreased dramatically, and after about 400 min, they disappeared. In the regime of dynamic coalescence, the mean size of both broken and coalesced mEP particles first (<10 min) increased rapidly, whereas later, it increased slowly. The observed morphological evolution was explained with the mechanism of phase evolution,[8,10,11] static coalescence,[24–27] and matrix film-drainage theory.[38,48]

Generally, we concluded that the evolution of the minor-phase particles across various regimes of the mPE/mEP (80/20 vol %) blend mixing was a result of interplay between their breakup and coalescence.

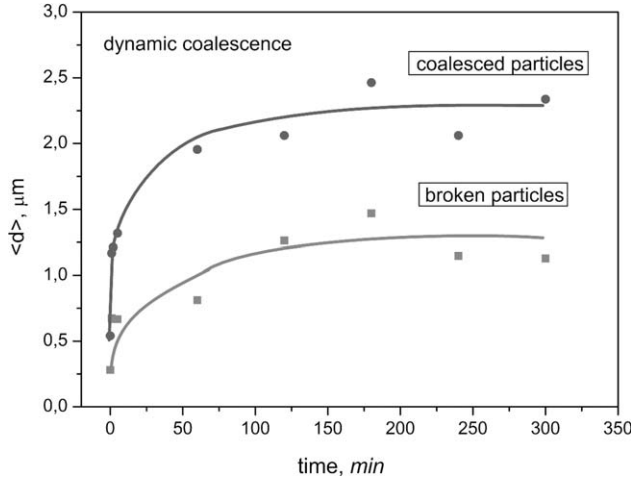

Figure 11. Variation of the mean diameter of the broken and coalesced mEP phase particles of the mPE/mEP blend with time during dynamic coalescence.

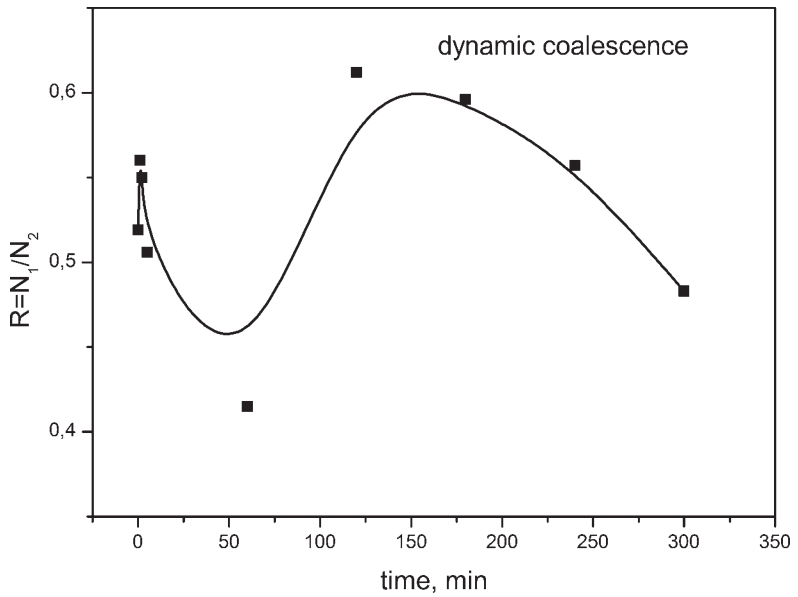

Figure 12. Variation of the ratio *R* between the numbers of broken and coalesced mEP phase particles with time during dynamic coalescence.

ACKNOWLEDGMENTS

The authors thank the Talent Foundation of Hubei University of Technology (contract grant number 2007D00001).

REFERENCES

1. Kayano, Y.; Keskkula, H.; Paul, D. R. *Polymer* **1997**, *38*, 1885.
2. Corte, L.; Beaume, F.; Leibler, L. *Polymer* **2005**, *46*, 2748.
3. Corte, L.; Leibler, L. *Polymer* **2005**, *46*, 6360.
4. Yin, B.; Zhao, Y.; Yu, R. Z.; An, H. N.; Yang, M. B. *Polym. Eng. Sci.* **2007**, *47*, 14.
5. Yang, X. D.; Zhu, Y. T.; Jiang, W. J. *Appl. Polym. Sci.* **2007**, *104*, 2690.
6. Schreiber, H. P.; Olguin, A. *Polym. Eng. Sci.* **1983**, *23*, 129.
7. Plochocki, A. P.; Dagli, S. S.; Andrews, R. D. *Polym. Eng. Sci.* **1990**, *30*, 741.
8. Scott, C. E.; Macosko, C. W. *Polym. Bull.* **1991**, *26*, 341.
9. Elemans, P. H. M.; Bos, H. L.; Janssen, J. M. H. *Chem. Eng. Sci.* **1993**, *48*, 267.
10. Scott, C. E.; Macosko, C. W. *Polymer* **1994**, *35*, 5422.
11. Scott, C. E.; Macosko, C. W. *Polymer* **1995**, *36*, 461.
12. Sundararaj, U.; Macosko, C. W. *Macromolecules* **1995**, *28*, 2647.
13. Sheng, J.; Qi, L. Y.; Yuan, X. B.; Shen, N. X.; Bian, D. C. J. *Appl. Polym. Sci.* **1997**, *64*, 2265.
14. Ratnagiri, R.; Scott, C. E. *Polym. Eng. Sci.* **1998**, *38*, 1751.
15. Yan, L. T.; Sheng, J. *Polymer* **2006**, *47*, 2894.
16. Li, Y. Y.; Hu, S. W.; Sheng, J. *Eur. Polym. J.* **2007**, *43*, 561.
17. Chen, X. H.; Ma, G. Q.; Li, J. Q.; Jiang, S. C.; Yuan, X. B.; Sheng, J. *Polymer* **2009**, *50*, 3347.
18. Hu, G. H.; Li, H. X.; Feng, L. F. *AIChE J.* **2002**, *48*, 2620.
19. Lifshitz, I. M.; Slyozov, V. V. J. *Phys. Chem. Solids* **1961**, *19*, 35.
20. Wagner, C. Z. *Elektrochem.* **1961**, *65*, 581.
21. Binder, K.; Stauffer, D. *Phys. Rev. Lett.* **1974**, *33*, 1006.
22. Siggia, E. D. *Phys. Rev. A* **1979**, *20*, 595.
23. Guo, H. F.; Packirisamy, S.; Mani, R. S.; Aronson, C. L.; Gvozdic, N. V.; Meier, D. J. *Polymer* **1998**, *39*, 2495.
24. Fortenly, I.; Kovar, J. *Polym. Compos.* **1988**, *9*, 119.
25. Fortelny, I.; Zivny, A. *Polymer* **1995**, *36*, 4113.
26. Fortelny, I.; Zivny, A. *Polymer* **1998**, *39*, 2669.
27. Fortelny, I.; Zivny, A.; Juza, J. J. *Polym. Sci. Part B: Polym. Phys.* **1999**, *37*, 181.
28. Yu, W.; Zhou, C. X.; Inoue, T. J. *Polym. Sci. Part B: Polym. Phys.* **2000**, *38*, 2378.
29. Yu, W.; Zhou, C. X.; Inoue, T. J. *Polym. Sci. Part B: Polym. Phys.* **2000**, *38*, 2390.
30. Vinckier, I.; Moldenaers, P.; Terracciano, A. M.; Grizzuti, N. *AIChE J.* **1998**, *44*, 951.
31. Kim, J. R.; Jamieson, A. M.; Hudson, S. D.; Manas-Zloczower, I.; Ishida, H. *Macromolecules* **1998**, *31*, 5383.
32. Lyu, S. P.; Bates, F. S.; Macosko, C. W. *AIChE J.* **2000**, *46*, 229.
33. Lyu, S. P.; Bates, F. S.; Macosko, C. W. *AIChE J.* **2002**, *48*, 7.
34. Rusu, D.; Peuvrel-Disdier, E. J. *Rheol.* **1999**, *43*, 1391.
35. Börschig, C.; Fries, B.; Gronski, W.; Weis, C.; Friedrich, C. *Polymer* **2000**, *41*, 3029.
36. Li, Y. Y.; Chen, Z. Q.; Huang, Y.; Sheng, J. J. *Appl. Polym. Sci.* **2007**, *104*, 666.
37. von Smoluchowski, M. *Phys. Chem.* **1917**, *92*, 129.
38. Chesters, A. K. *Chem. Eng. Res. Des.* **1991**, *69*, 259.
39. Zeichner, G. R.; Schowalter, W. R. *AIChE J.* **1977**, *23*, 243.

40. Wang, H.; Zinchenko, A. Z.; Davis, R. H. J. *Fluid Mech.* **1994**, *265*, 161.
41. Kilian, H. G.; Zink, B.; Metzler, R. J. *Chem. Phys.* **1997**, *107*, 8697.
42. Kilian, H. G.; Bronnikov, S.; Sukhanova, T. J. *Phys. Chem. B* **2003**, *107*, 13575.
43. Bronnikov, S.; Dierking, I. *Phys. Chem. Chem. Phys.* **2004**, *6*, 1745.
44. Zuev, V. V.; Bronnikov, S. J. *Polym. Res.* **2010**, *17*, 731.
45. Zuev, V. V.; Steinhoff, B.; Bronnikov, S.; Kothe, H.; Alig, I. *Polymer* **2012**, *53*, 755.
46. Zuev, V. V.; Bronnikov, S. J. *Macromol. Sci. Part B: Phys.* **2012**, *51*, 1558.
47. Mousa, H.; Agterof, W.; Mellema, J. J. *Colloid Interface Sci.* **2001**, *240*, 340.
48. Janssen, J. M. H.; Meijer, H. E. H. *Polym. Eng. Sci.* **1995**, *35*, 1766.